

## General Disclaimer

### One or more of the Following Statements may affect this Document

- This document has been reproduced from the best copy furnished by the organizational source. It is being released in the interest of making available as much information as possible.
- This document may contain data, which exceeds the sheet parameters. It was furnished in this condition by the organizational source and is the best copy available.
- This document may contain tone-on-tone or color graphs, charts and/or pictures, which have been reproduced in black and white.
- This document is paginated as submitted by the original source.
- Portions of this document are not fully legible due to the historical nature of some of the material. However, it is the best reproduction available from the original submission.

(NASA-TM-84946) INTERPLANETARY RADIO  
STORMS. 2: EMISSION LEVELS AND SOLAR WIND  
SPEED IN THE RANGE 0.05-0.8 AU (NASA) 34 p  
HC A03/MF A01 CSCL 03B

N85-13761

Unclass

83/92 12486



## Technical Memorandum 84946

# INTERPLANETARY RADIO STORMS: 2 - EMISSION LEVELS AND SOLAR WIND SPEED IN THE RANGE 0.05 - 0.8 AU

RECEIVED  
A.I.A.A.  
1983 SEP 12 PM 3:33  
T. I. S. LIBRARY

J.-L. Bougeret, J. Fainberg and R. G. Stone

DECEMBER 1982

National Aeronautics and  
Space Administration

**Goddard Space Flight Center**  
Greenbelt, Maryland 20771



INTERPLANETARY RADIO STORMS.  
2: EMISSION LEVELS AND SOLAR WIND SPEED  
IN THE RANGE 0.05-0.8 AU

J.-L. Bougeret(\*), J. Fainberg, and R. G. Stone  
NASA/Goddard Space Flight Center  
Laboratory for Extraterrestrial Physics  
Greenbelt, MD 20771, U.S.A.

(\*) NAS/NRC Postdoctoral Research Associate on leave from Laboratory  
Associated with CNRS # 264, Paris Observatory, France.

to be submitted to: Astronomy and Astrophysics

## ABSTRACT

Storms of interplanetary type III radio bursts (IP storms) are commonly observed in the interplanetary medium by the ISEE-3 radio instrument. This instrument has the capability of accurately determining the arrival direction of the radio emission. At each observing frequency, the storm radio sources are tracked as they cross the line-of-sight to the Sun. Using a simple model, the emission levels are determined at a number of radio frequencies for four separate storms. The IP storm radiation is found to occur in regions of enhanced density at levels of 0.05-0.8 AU. The density in these enhancements falls off faster than  $R^{-2}$ . The solar wind speed in the storm region is also measured. The analysis is consistent with steady conditions in the storm region during a few days around the central meridian passage of the storm. The comparison with average in situ density measurements compiled from the HELIOS 1-2 observations favors type III storm burst radio emission at the harmonic of the local plasma frequency.

## INTRODUCTION

Long duration storms of type III radio bursts were discovered in the hectometer wavelength range during the last solar cycle, utilizing the RAE-1 satellite observations. Some of their characteristics have been investigated by Fainberg and Stone (1970a,b; 1971a,b) who analyzed extensively the storm of August 1968. The type III storms are characterized by a quasi-continuous production of fast drift bursts which persist over an observing period of half a solar rotation. A peak value of 360 storm bursts per hour has been observed at 2.8 MHz. The number of bursts observed per hour decreases with frequency, which is essentially due to the increase of the duration of the type III bursts with decreasing frequency (e.g. Evans et al., 1973). The observed activity is maximum near central meridian passage (CMP). This is understood as a consequence of a combination of radiation beaming and the influence of the medium on the propagation of radiation from source to observer.

The type III drift rate dependence on solar longitude has been analyzed by Fainberg and Stone (1970a,b) during the storm of August 1968. The drift rate dependence is shown to be a consequence of the propagation time of emission from the source to the observer. Based on this dependence, an average exciter speed of 0.38 c was deduced for the height range from approximately 11 to 30 solar radii ( $R_{\odot}$ ). From the same data, Fainberg and Stone (1971a) deduced a distance scale between plasma levels in the storm region, an upper limit to the scale size of coronal density inhomogeneities, and an estimate of the solar wind speed in the storm region. By assuming the electron density at a given plasma level, the distance scale was used to derive the coronal density model:  $N_e = 5.52 \cdot 10^7 R^{-2.63}$ , where  $N_e$  is the electron density in  $\text{cm}^{-3}$ , and  $R$  the heliocentric distance in  $R_{\odot}$ . This model is sometimes referred to in the literature as the RAE model.

In a previous paper (Bougeret, Fainberg, and Stone, 1983a, hereafter paper 1), we have shown that the storms of interplanetary type III radio bursts (in short IP storms) may occur at a rate of 2 to 3 per solar rotation in a period of solar maximum, and may last from 1 to 12 days. They are closely related to the solar active regions, and appear to be the extension into the interplanetary space up to 100-170  $R_{\odot}$  of the meter wave type I and type III storm activity.

In this paper we utilize the spinning dipole technique (Fainberg et al., 1972) which yields the source solar elongation. The long duration of the storm enables us to track the storm sources as they corotate with the Sun, during several consecutive days. The resulting geometrical effect provides information on the distance of the source from the observer (or the Sun). We use the observations of the Paris Observatory/NASA Goddard Space Flight Center radio mapping experiment on board the ISEE-3 spacecraft (Knoll et al., 1978). Besides its direction finding capability over a wide range of frequencies (2 MHz-30 kHz), this instrument is particularly good for the study of weak and long lasting phenomena such as the radio storms for two main reasons. Firstly it has a very high sensitivity ( $10^{-21}$ - $10^{-20}$  W m<sup>-2</sup> Hz<sup>-1</sup>) and is interference free. Secondly its location at the libration point towards the Sun considerably reduces interference from the Earth's radio noise (TKR) and allows almost continuous observations.

#### THE ISEE-3 RADIO DATA

The ISEE-3 radio mapping experiment has been described briefly in paper 1. A more complete description of the experiment is given by Knoll et al. (1978). In what follows we discuss briefly the technique which enables us to obtain the parameters which we have utilized to study the IP storms. We have used the measurements from the dipole antenna (90 m tip to tip) which is in the spin plane and rotates with the spacecraft (1 rotation in approximately 3 s). Figure 1 shows the modulation of the antenna temperature T at a given radio frequency produced by a compact solar radio source during half a spacecraft rotation (a dipole antenna has a 180° ambiguity). The data acquisition rate is such that about 11 independent measurements are made during each half rotation. For each observing frequency these 11 measurements are least-squares fitted with a sine wave, from which we deduce three parameters:

(1) the maximum value ( $T_{\max}$ ) which is the level of the signal we would expect to see if the dipole antenna axis were perpendicular to the direction of the source centroid (direction of maximum antenna gain). This maximum value is defined as the "despun" value of the temperature and is used to compute the flux density of the radio emission (see Appendix).

(2) The phase of the sine wave, which gives the arrival direction in the ecliptic plane or azimuth (hereafter source solar elongation) of the source centroid and is referred to as the  $\phi$  angle (negative East, positive West).

(3) The minimum value ( $T_{\min}$ ) which is the minimum antenna temperature we would expect to see if the dipole antenna axis were pointed to the source centroid (direction of minimum antenna gain).  $T_{\max}$  and  $T_{\min}$  are used to define the modulation index  $\alpha$ , using the expression  $\alpha = (T_{\max} - T_{\min}) / (T_{\max} + T_{\min})$ . This index  $\alpha$  is further used to estimate the radio source angular size, assuming a brightness distribution for the source (Fainberg, 1979).

These three parameters, namely the despun antenna temperature, the solar elongation  $\phi$  and the modulation index  $\alpha$  are shown in Fig. 2 for a given frequency and for one hour when an isolated type III burst is observed. Each data point on this Figure is the result of the least-squares analysis of 11 basic measurements as shown in Fig. 1. The 24 radio frequencies available on the ISEE-3 radio instrument are sampled according to a frequency stepping sequence discussed by Knoll *et al.* (1978), which permits increased time resolution at higher frequencies, within the available telemetry rate.

Using time averages of the intensities we have produced gray shaded dynamic spectra as shown in Fig. 3. The lower panel shows 10 days of storm activity and the upper panel is a six hour blow up. The individual type III storm bursts can be distinguished on the high resolution plot, but not on the 10 day plot which exhibits a continuous band of emission characteristic of IP storms.

### THE IP STORM DATA ANALYSIS TECHNIQUE

#### The 30 minute average data

The observed lifetimes of the IP storms range from 1 to 12 days (paper 1). This is very long compared to the time resolution of the ISEE-3 radio experiment which ranges from 12 measurements of intensity,  $\phi$ , and  $\alpha$  per data analysis cycle (54 s) for the highest frequency (1980 kHz) to 1 measurement per data analysis cycle for the lowest frequency (30 kHz). As an example, Figure 4 shows the time

variation of the (despun) flux density for three hours of storm activity at 3 frequencies (1000, 466, and 145 kHz). In order to reduce the amount of data which is processed, and to describe the general behavior of the storm rather than that of the individual bursts, we have chosen to use 30 min. averages of the measured parameters: the logarithm of the flux density, the source solar elongation  $\phi$  (azimuth in the ecliptic plane) of the radio emission and the modulation index  $\alpha$ . For each parameter, the average, and the r.m.s. deviation have been computed for each 30 min. interval. We have also kept the minimum of the flux density observed during each 30 min. interval. As already shown, (Fainberg and Stone, 1971b; paper 1) the minimum radio flux does not drop to the background level during an IP storm. Therefore the curve of the minima describes the lower envelope of the storm activity with a 30 min. resolution. The averages and the minima are indicated respectively by circles and crosses on Fig. 4. At the higher frequencies the  $F_{\min}$  profile is much less noisy than the averaged flux density profiles essentially because more intense type III bursts which do not belong to the storm and are shorter than 30 min. are removed. This is illustrated in the second half of Fig. 4 where the more intense, non-storm type III burst contributes to a higher average, but does not affect the 30 min. minimum flux at 1000 kHz and 466 kHz.

Geometric averages of the intensities (averages of the logarithms of the despun intensities) have been calculated rather than arithmetic averages for the following reasons: 1) the radio receiver has a logarithmic response in intensity in order to cover the very large dynamic range of the interplanetary radio bursts (sometimes larger than 70 dB); 2) the noise follows a logarithmic law since  $\Delta T/T$  is about constant ( $T$  is the noise temperature measured by the receiver,  $\Delta T$  is the measurement accuracy); 3) even for the IP storms (which have a typical dynamic range of 20 dB or less), averaging the linear intensities would favor the stronger bursts, and would not account for the bulk of the events which have smaller intensities.

The comparison of the minimum values, the average values and the r.m.s. deviations at a given frequency provides a good description of the "variability" of the signal at that frequency, in a way similar to that used for the type I radio storms. For instance the variability is found to be lower during an IP storm than during an accumulation of individual, flare related type III bursts observed at the same frequency.



### The galactic background subtraction

Figure 5a shows the time variation of the 30 min. averages of the logarithm of the flux density at a variety of frequencies. The background level for the higher frequencies is essentially the galactic background (Fig. 3 of paper 1). This background has been subtracted (Fig. 5b) using procedures explained in the Appendix. In what follows it will always be subtracted, unless otherwise noted. Fig. 5c shows the same storm as described by the 30 min. minima. It is clearly seen that the maximum flux density occurs later and later as the frequency decreases; this frequency drift is also seen in Fig. 3 and will be interpreted as an effect of directivity in a forthcoming paper.

### The source solar elongation variation

Figure 6 shows the time variation of the solar elongation  $\phi$  at a variety of frequencies for the same storm. The elongation is corrected for the galactic background contribution (see Appendix). This Figure illustrates some of the major, new contributions of the ISEE-3 radio experiment to the observation of the IP storms reported in this series of papers. Several main points can be deduced from this Figure:

(1) These data provide the first direct evidence that all the type III storm bursts are emitted within the same region. As a matter of fact this stability and small scatter of the elongations (positions) of the centroids of the radio source has been used as a necessary condition to define an IP storm. It is clearly different from a large number of flare-related type III bursts which are usually much more scattered in position.

(2) The radio source is tracked for several days from the East to the West: it is observed to corotate with the Sun during the course of the storm. The steeper slopes at lower frequencies reflect the increasing distance of the source from the Sun: the lower the frequency the closer the source is to the observer who observes it crossing his line-of-sight more rapidly. We measure the slope  $\phi' = d\phi/dt$  of the source solar elongation variation (the source elongation rate) around the central meridian passage (CMP) (Fig. 7). Assuming that the storm region rotates rigidly

with the Sun (steady state hypothesis), and knowing the rotation rate  $\Omega$ , the emission levels  $R$  can be deduced at each frequency; if the source is situated in the ecliptic plane, we immediately find

$$R = D \phi' / (\Omega + \phi');$$

where  $D$  is the distance from the Sun to the spacecraft. Such a technique has already been used in ground-based solar radio astronomy (see for instance Gergely and Kundu, 1975), but it has never reached such a quality because of the much lower time coverage of the ground-based observations.

(3) The time of CMP which is defined as the time when the radio source is observed to cross the direction of the Sun is observed to occur later when the frequency is lower. This is interpreted as the result of the radio source being located along a curved trajectory of the large scale magnetic field as shown on Fig. 7.

#### Uncertainties in the determination of the emission levels

We note that the source solar elongation rate is measured around CMP. This helps reduce possible scattering or refraction effects, which are likely to be more important at larger longitudes. In order to further check such effects, we have also verified that the modulation index  $\alpha$  does not show significant fluctuations around CMP; this is not always true at the larger longitudes.

The source centroids are assumed to be located close to the ecliptic plane. This assumption will be checked by direct measurement of the source elevation angles to be presented in a forthcoming paper. We find that the distances of the emission levels to the Sun will be underestimated by no more than 5%, if the storm centroid trajectory makes an angle of less than  $15^\circ$  to the ecliptic plane. Furthermore, for distances smaller than 0.5 AU, the different emission levels are affected by almost the same relative error, thus having minor effect on the exponent of the emission level scale which will be discussed in the next Section.

The solar rotation rate is known to vary with latitude (differential rotation) and somewhat with time during the course of the solar cycle. We have considered a uniform value of  $13.2^\circ \text{ d}^{-1}$  (1 rotation in 27.275d). An underestimation of 8% on

this value (1 true rotation in 25d) yields a 4% underestimation of the emission level at 0.5 AU. The exponent of the emission level scale is underestimated by a similar amount. In a future analysis, we plan to use the true rotation rate of the associated active region whenever identifiable.

## RESULTS

### The emission levels

Figure 8 shows the emission levels measured for four storms. Each storm on this log-log plot is roughly a straight line and can be described by two parameters; a coefficient and a slope (power law index of the emission level scale). A slope of  $-1$  corresponds to  $-2$  in a log-log electron density-distance plot, since the plasma frequency is proportional to the square root of the electron density. The thin line in Figure 8 shows the best fit to the four storms. The heavy black line are levels deduced from the first radio storm observed by RAE-1 (Fainberg and Stone, 1971a). By contrast, for this previous analysis and as discussed earlier, it was necessary to assume the emission level at a given frequency. The results from different techniques, however, are in excellent agreement. As was already found in the RAE observations, the slope is significantly steeper than  $-1$  (which corresponds to a falloff steeper than  $-2$  for the electron density). Observations of type III storms in the lower corona (Gergely and Kundu, 1975) are also shown on the same Figure. They are in good agreement with the extrapolation of the ISEE-3 observations to the higher frequencies. For the lower frequencies, the comparison with the in-situ plasma measurements (HELIOS 1-2) will be discussed in the next section.

### Solar wind speed

Figure 9 shows an example of the trajectory of the storm as deduced from the measurement of both the emission level and the time of CMP. This determination does not require any hypothesis on the radiation mode. The technique has been described in detail elsewhere (Bougeret, Fainberg, and Stone, 1983b) and it enables us to track remotely the element of plasma responsible for the radio waves

as it is convected outward by the solar wind and thus yields an estimate of the solar wind speed in the direction of the Earth. The results are very close to an Archimedean spiral which is also shown on the Figure. The average solar wind speed for this storm is  $270 \text{ km s}^{-1}$ . It shows a slight solar wind acceleration similar to that found by Bougeret et al. (1983b). Taking into account this acceleration, the extrapolated speed at 1 AU is  $380 \text{ km s}^{-1}$ . For the 4 storms that are presented in this paper, the spiral shape is compatible with solar wind speeds in the range  $250\text{--}600 \text{ km s}^{-1}$  (Table 1).

## DISCUSSION

### The steady state model

Assuming the density model and the solar wind speed as measured around CMP, it is easy to predict the variation of the source solar elongation several days before and after the CMP. Figure 10 shows the fit of this simple model to the storm shown in Fig. 6. It shows that we can account for the observation with a steady state model of solar wind in the storm region, in which conditions -electron density and solar wind speed- are uniform for 4 or 5 days. Since the IP storm is closely related to the solar active region (paper 1), this means that the extension of the active region through the interplanetary medium is quasi-steady, on a large scale, for a period of at least 4 or 5 days. This behavior is found in the other 3 storms that are mentioned on Fig. 8 and Table 1, and was also inferred by Fainberg and Stone (1970b) for the August 1968 storm. However, Fig. 10 shows that the observations depart from the steady state model at the larger elongations. This could indicate either variations in the density model and/or solar wind speed, or could be due to increased propagation effects at the limbs.

### The type III storm bursts trajectory

The scatter of the 30 minute averages of the source solar elongation about the model is remarkably small (Figs. 6 and 10). The r.m.s. deviations in each 30 minute period is also very small. This dispersion, along the path of the bursts, increases as distance from the Sun, and the centroids are scattered in an angle of

less than 2 to 3 degrees as seen from the Sun. This is of course much smaller than the source size which is estimated to correspond to an angle of about 30 to 40 degrees (as seen from the Sun) for this same storm. Together with the steady state model mentioned above, this means that the trajectories of the individual storm bursts are very similar in a reference system tied to the Sun: the electron packets responsible for the radio emission must travel along a very well determined magnetic path, characteristic of each storm.

The storm shown in Fig. 6 is one for which the scatter of the centroids of the radio sources has been found to be the smallest. The scatter of the source centroids of other storms is not much larger and is usually less than 5 degrees. As already mentioned the condition that a given source can be tracked for at least 1 day has been set as a necessary condition to define an IP storm. A very small (less than 5 degrees as seen from the Sun) scatter of the 30 minutes averages of the solar elongation around an empirical average curve is also a necessary condition to define a storm. The 4 storms that are presented in this paper are "simple" in the sense that all the type III storm bursts seem to describe the same trajectory. Just as the type I storms may consist of several distinct sources within the same storm region (Eougeret, 1971), the IP storms may consist of exciter trajectories along several paths, which may account for the larger scatter or irregular variation of the source centroids of some storms which are henceforth described as "multiple". The ISEE-3 observations show that about one storm out of five presents a regularly drifting source solar elongation profile, sufficient to perform the analysis as explained in the previous sections. The other storms show good evidence for the existence of multiple sources which cannot be resolved (the radio experiment measures only the centroid and the source size).

#### Emission levels and solar wind electron density

In principle, if the radiation mode of the type III emission were known (fundamental or harmonic of the local plasma frequency) the density scale could be readily deduced from the emission level scale: the frequency scale on Fig. 7 could be replaced by a scale in  $9 N_e^{1/2}$  (fundamental hypothesis), or  $18 N_e^{1/2}$  (harmonic hypothesis) ( $N_e$  in  $\text{cm}^{-3}$  and frequency in kHz). However, one has also to consider the large size of the IP storm sources: typically of 30 to 50 degrees as seen from

the Sun, which represents about 0.25-0.45 AU at 0.5 AU (work in progress), clearly much larger than the likely interplanetary structures. Scattering of the electromagnetic radiation on electron density inhomogeneities is likely to contribute significantly to this size. For example, the scattered image of a point source observed at 110 kHz and located at 0.5 AU may have an apparent size close to  $40^\circ$  when observed from 1 AU (Hornstein, private communication). In the following, we discuss some effects that are expected if the observed size is close to the true size. For a source observed at a given frequency, the narrow bandwidth of the receiver suggests a very small thickness of the source along the solar radial (direction of the density gradient). But this may be only true locally: at a given distance from the Sun, the electron density is likely to vary by large amounts over areas of 0.25-0.45 AU, resulting in an overall radial extension of the source much larger than that determined by the receiver bandwidth alone. For instance, a deviation  $\Delta N_e$  of the order of  $N_e$  in the source area could account for an overall thickness of the source of the order of its lateral extent. Such large density fluctuations do not occur randomly in the interplanetary medium, but rather follow large scale structures. Hence it is more likely that the source is distorted radially in a more or less organized way. If that is the case (and it is likely to be the case since the IP storms are associated with regions of enhanced density as will be discussed lower), our analysis provides an average measure of the emission level over a large volume (the source volume) which obviously also extends out of the ecliptic plane.

In the following we discuss how this averaging will affect the slope of the emission level scale presented in the previous section. It can be easily shown that if (i) the degree of large scale inhomogeneity remains constant with increasing distance from the Sun, and (ii) the source size is constant as seen from the Sun, a slope in the density model steeper than  $R^{-2}$  cannot be artificially created by the averaging effects. On the other hand a decrease steeper than  $R^{-2}$  could be artificially created even if the density were everywhere proportional to  $R^{-2}$ , if the source size were to increase faster than  $R$  (there is no evidence for that up to now), or if the degree of inhomogeneity were to decrease with increasing distance from the Sun. We are not in a position to discuss this problem thoroughly in this paper.

### Comparison to in-situ measurements and radiation mode

The 2 parallel lines in Fig. 8 (labelled HELIOS 1-2) are deduced from in situ measurements of the solar wind plasma computed by Bougeret, King, and Schwenn (1983c) from the plasma experiments on HELIOS 1 and 2 (Rosenbauer et al., 1977). The data have been averaged from 1974 to 1980 and normalized year by year to the average density at 1 AU in order to remove solar cycle fluctuations. The density model normalized to 1976 is:  $N_e = 6.14 R^{-2.10}$  where the density is in  $\text{cm}^{-3}$  and the distance in AU. The range of distances covered is 0.3 to 1 AU. Since the ordinate in Figure 8 is frequency, we have converted the plasma densities in plasma frequencies and the second harmonic of the plasma frequency.

We note that the continuity of the frequency-distance curve observed for each storm implies that the same mode pervades certainly throughout the frequency domain analyzed. Our observations tend to be more consistent with the harmonic of the plasma frequency. An emission on the fundamental mode would imply densities in the storm region (extrapolated to 1 AU) more than 4 times larger than the average. Even if one assumes that the harmonic mode is radiated, the IP storm is obviously emitted in overdense regions. These regions are even denser closer to the Sun, as can be seen from Table 1 which compares the storm densities to the HELIOS densities at two distances from the Sun (0.1 AU and 1 AU) in the harmonic hypothesis. Our observation is more consistent with the harmonic hypothesis. A comparison of the densities extrapolated to 1 AU to the in-situ measurements of the plasma experiment on board ISEE-3, at times when the extrapolation of the storms were expected to hit the spacecraft shows that this hypothesis is reasonable; the fundamental would lead to too large densities.

### CONCLUSION

We have presented new results on the interplanetary type III radio storms (IP storms). The major progress is due to the spinning antenna technique which enables us to determine the solar elongation and apparent size of the IP storm sources. The long duration of the IP storms combined with the solar rotation enables us to determine the emission levels of the frequencies at which the storms are observed. The IP storms can be observed from 1980 kHz (upper limit of the ISEE-3 radio

experiment band) down to frequencies of 110 kHz, sometimes less (80 kHz) which covers a range of distances from the Sun of 0.05 AU to 0.8 AU (10-175  $R_{\odot}$ ). Results have been presented for 4 storms. The emission level scale and the solar wind speed have been deduced for each storm. The results are in very good agreement with earlier results from the RAE satellite, which used a different technique. Our technique requires fewer hypotheses. Comparison with in-situ plasma density measurements supports a radiation at the harmonic of the plasma frequency.

Assuming that the radio source describes an average volume of plasma in the storm region, the emission level scale can be readily taken as an average density scale in the IP storm region. The exponent of the density dependence on distance is smaller than -2 which is expected for a constant, spherically symmetric solar wind expansion. The exponents average to -2.8 for the 4 storms presented in this paper. We deduce from this result that the IP storms occur in regions which are denser than the ambient solar wind and where the density decreases faster than  $R^{-2}$ . The extrapolation of the densities in these regions back to the Sun connects well to the decameter and meter wavelength observations of the type III storms. The 4 storms presented in this paper are simple in the sense that all the type III bursts that constitute them follow the same trajectory during 4 or 5 days. This trajectory is very close to an Archimedean spiral and its pitch yields the solar wind velocity in the storm region. For 3 storms out of 4 the velocities are in the range 250-300  $\text{km s}^{-1}$ . The stationarity of the conditions in the storm region and the small scatter of the centroids around the average position are a clear demonstration that the energetic electrons responsible for the IP storm emission have to follow the IP magnetic field lines which are hence relatively stable in the course of the storm (within the storm region.)

In conclusion, the IP storms present properties which are unique and distinct from the non-storm type III bursts. They describe unique large scale, overdense structures in the interplanetary medium which are closely associated to the solar active region and are very likely the extension of coronal streamers through the interplanetary medium.



APPENDIXConversion to flux density and galactic background subtraction

The calibration of the ISEE-3 radio experiment is accomplished by switching a noise generator in the preamplifiers and stepping through six different noise levels for each radiometer frequency covering 60 dB of the dynamic range (Knoll et al., 1978). The receiver temperature was obtained from measurements made before the antenna was deployed. The noise levels are continuously monitored to check for gain variation of the receiver. The receiver noise temperature is first subtracted from the antenna temperature  $T$ . Then this corrected temperature is converted to flux density according to the expression (Kraus, 1966):

$$S = 2 k T / A_e \quad (1),$$

where  $S$  = flux density,  $W m^{-2} Hz^{-1}$ ;  $k = 1.38 \cdot 10^{-23}$  joule  $K^{-1}$ , the Boltzmann's constant;  $A_e$  = effective aperture,  $m^2$  given by:

$$A_e = G \lambda^2 / 4 \pi \quad (2),$$

where  $\lambda$  = wavelength,  $m$ ;  $G = 3 / 2$  (dipole antenna).

As can be seen on Fig. 4 of paper 1 the sensitivity of the radiometer is limited by the galactic background above  $\sim 150$  kHz and by the thermal noise on the antenna below  $\sim 150$  kHz. The latter noise depends on the solar wind plasma density and temperature and cannot be subtracted easily since it is usually variable, sometimes within minutes (Hoang et al., 1980). On the other hand the galactic background is a constant source of noise which can be systematically subtracted since it appears as a modulated background component and can thus be analyzed. Such a subtraction not only helps detect small bursts out of the noise, but it is also critical to the accurate determination of the direction of arrival of weak radio emissions such as that from the IP storms studied in this series of papers.

The galactic background has been measured at times when no activity was observed either on the Sun or on the Earth (TKR). The sensitivity of the ISEE-3 radio instrument is such that very few such periods have been found on the 30 min. average data. We have performed a systematic search for flux density minima and checked the absence of activity on high time resolution intensity plots and dynamic spectra. For each quiet period retained, we have measured the 30 min. average values of the flux density, the source solar elongation  $\phi$ , and the

modulation index  $\alpha$ . The 30 min. average of the background flux density is found to be constant over the period studied (Aug. 78-Jan. 80) within 0.005 dB (0.1%) at 1980 kHz, and 0.03 dB (0.6%) at 233 kHz. This confirms the long term stability of the receiver.

The solar elongation of the galactic background is found to be approximately the same for the different frequencies above about 200 kHz for which it can be easily detected. Below this frequency, terrestrial and thermal noise make the accurate measurement of  $\phi$  and  $\alpha$  difficult from the 30 min. average data. The value of  $\phi$  measured during quiet periods are shown on Figure A1 from August 1978 to January 1980. The 6 month periodicity results from the  $180^\circ$  ambiguity of the dipole antenna. The least-squares fit of the measurements to a straight line has provided a simple formula to find the galactic background direction at any time. Its right-ascension (in equatorial coordinates) is found to be approximately 11 h 42 m  $\pm$  12 h which is quite comparable to previous results obtained by Brown (1973). This measurement obviously includes contributions from the Galaxy as a whole and other bright radio sources. It is different from the direction of the galactic nucleus because of the strong absorption present in this frequency range (Alexander and Novaco, 1974). Indeed the observed modulation index is low ( $\alpha \sim 0.16-0.18$ ) as expected for a broad source (such a value of  $\alpha$  is obtained with a circular gaussian shaped source centered in the ecliptic plane and having a half power width of about  $70^\circ$ ).

The galactic background component is removed in the following way (Fainberg, 1979). Let  $S_0$ ,  $\alpha_0$ , and  $\phi_0$  be the average flux density, modulation index, and solar elongation of the background, as determined during the quiet periods, and let  $S_1$ ,  $\alpha_1$ , and  $\phi_1$  be the measured average flux density, modulation index, and elongation of the burst source plus background. Fainberg (1979) has obtained the following expressions for the quantities characterizing the burst source alone:  $S_b$ ,  $\alpha_b$ , and  $\phi_b$ :

$$S_b = S_1 - S_0 \quad (3)$$

$$\alpha_b = \{ [(\alpha_1 S_1)^2 + (\alpha_0 S_0)^2 - 2\alpha_1 \alpha_0 S_1 S_0 \cos 2(\phi_1 - \phi_0)] / (S_1 - S_0) \}^{1/2} \quad (4)$$

$$\tan 2\phi_b = [\alpha_1 S_1 \sin 2\phi_1 - \alpha_0 S_0 \sin 2\phi_0] / [\alpha_1 S_1 \cos 2\phi_1 - \alpha_0 S_0 \cos 2\phi_0] \quad (5)$$

References

- Alexander, J.K., and Novaco, J.C.: 1974, Astron. J. 79, 777
- Bougeret, J.-L.: 1973, Astron. Astrophys. 24, 53
- Bougeret, J.-L., Fainberg, J., and Stone, R.G.: 1983a, Astron. Astrophys., paper 1, (in press)
- Bougeret, J.-L., Fainberg, J., and Stone, R.G.: 1983b, Science (in press)
- Bougeret, J.-L., King, J.H., and Schwenn, R.: 1983c, to be submitted to Astron. Astrophys.
- Brown, L.W.: 1973, Astrophys. J. 180, 359
- Evans, L.G., Fainberg, J., and Stone, R.G.: 1973, Solar Phys. 31, 501
- Fainberg, J.: 1979, NASA Technical Memorandum 80598, NASA/GSFC, Greenbelt, Maryland 20771, U.S.A.
- Fainberg, J., and Stone, R.G.: 1970a, Solar Phys. 15, 222
- Fainberg, J., and Stone, R.G.: 1970b, Solar Phys. 15, 433
- Fainberg, J., and Stone, R.G.: 1971a, Solar Phys. 17, 392
- Fainberg, J., and Stone, R.G.: 1971b, Astrophys. J. 164, L123
- Fainberg, J., Evans, L.G., and Stone, R.G.: 1972, Science 178, 743
- Gergely, T.E., and Kundu, M.R.: 1975, Solar Phys. 41, 163
- Knoll, R., Epstein, G., Hoang, S., Huntzinger, G., Steinberg, J.-L., Fainberg, J., Grena, F., Mosier, S.R., and Stone R.G.: 1978, IEEE GE-16, 199
- Manning, R., and Fainberg, J.: 1979, Space Sci. Instrum. 5, 161
- Rosenbauer, H., Schwenn, R., Marsh, E., Meyer, B., Miggenrieder, H., Montgomery, M.D., Mulhauser, K.-H., Philipp, W., Voges, W., and Zink, S.M.: 1977, J. Geophys. 42, 561
- Wild, J.P., and Smerd, S.F.: 1972, Ain. Rev. Astron. Astrophys. 10, 159

FIGURE CAPTIONSFigure 1:

The 11 elementary measurements taken at one radio frequency over half a spacecraft rotation. The sine wave is least-squares fitted and yields the despun intensity, the solar elongation and the size of a compact radio source as explained in the text.

Figure 2:

The intensity (antenna temperature), solar elongation  $\phi$  and modulation index  $\alpha$  derived from the spin analysis during an isolated type III burst observed at 513 kHz. Each data point on this plot results from the least-squares analysis of 11 points as shown in Figure 1. 23 different radio frequencies are available on ISEE-3.

Figure 3:

10 day dynamic spectrum (middle panel), and 12 hour blow-up (upper and lower panel) of an IP storm observed by the ISEE-3 radio experiment. Individual storm bursts can be identified on the 12 hour gray-shaded plot (see upper panel), while the 10 day plot gives an appearance of continuity. A few isolated type III bursts can be identified in the lower panel and compared to the smaller type III storm bursts. The overall frequency drift of the storm (see also Fig. 5) will be interpreted in a forthcoming paper.

Figure 4:

Example of type III storm activity observed at the standard time resolution. Several tens of individual type III storm bursts can be identified on the high frequency channel. The typical duration of the bursts is of 1-2 min. at 1000 kHz. The burst duration varies as  $f^{-1}$  (Evans et al., 1973) resulting in a time profile which is smoother for lower frequencies. A large type III burst, not related to the storm, is also seen starting around 10:00 at 1000 kHz and occurring later at lower frequencies. It is more intense than the typical storm bursts, especially at the lower frequencies. We find that its elongation is clearly different from that of the storm bursts. The 30 min. averages are shown by open circles, and the 30 min. minima by crosses.

Figure 5:

Example of 30 min. average or minimum values of the flux density as a function of time for 5 of the 24 frequencies available on ISEE-3, during an IP storm. (a) 30 min. average of the flux density. The background is the galactic noise. (b) 30 min. averages of the flux density after subtraction of the galactic background (see Appendix). (c) 30 min. minimum of the flux density with galactic background subtraction. These last time profiles are much cleaner, since sporadic bursts, unrelated to the storm are removed, as explained in the text (see Fig. 3).

Figure 6:

Time variation of the source solar elongation for the storm of May 31-June 5, 1979. At each frequency the drift is produced by the solar rotation and it is faster ~~for~~ for lower frequencies since the radio source is closer to the observer. The time of CMP occurs later at lower frequencies reflecting the spiral shape of the magnetic field lines (see Fig. 7). The time resolution on this plot is 30 minutes.

Figure 7:

Sketch illustrating the determination of the distance scale and spiral shape. During the time interval  $\Delta t$ , the source centroid moves from A to B by  $\Delta x$  while the Sun rotates by  $\Delta \omega$ . For a given frequency, we have  $\Delta x / \Delta t = R \Delta \omega / \Delta t = (D-R) \Delta \phi / \Delta t$ , from which R can be deduced. The observation at two different frequencies enables us to track two sources  $M_1$  and  $M_2$  along the electron path. Starting from the dashed spiral, CMP will be observed after a Sun rotation equal to  $\omega_1$  for  $M_1$ , and  $\omega_2$  for  $M_2$ , from which the spiral pitch (or solar wind speed) is deduced.

Figure 8:

Emission levels of 4 IP storms. The RAE model is also shown as well as observations of type III and type I storms at higher frequencies and in situ measurements by HELIOS 1 and 2 (after Bougeret et al., 1983c). A slope of -1 in this log-log frequency-distance scale corresponds to a slope of -2 in the log-log electron density-distance scale.

Figure 9:

Trajectory of the type III storm radio source as deduced from the radio observation for the storm of May 31-June 5, 1979 shown in Fig. 6.

Figure 10:

Source elongation expected for a steady state, stationary, corotating model superimposed on the observed elongation for 3 frequencies of the May 30-June 6, 1979 storm. The model is determined by (i) the density model (a factor and an exponent), (ii) the solar wind speed, and (iii) a time origin at a given distance. Those parameters are determined from the analysis of the storm during 1 or 2 days around CMP.

Appendix:Figure A1:

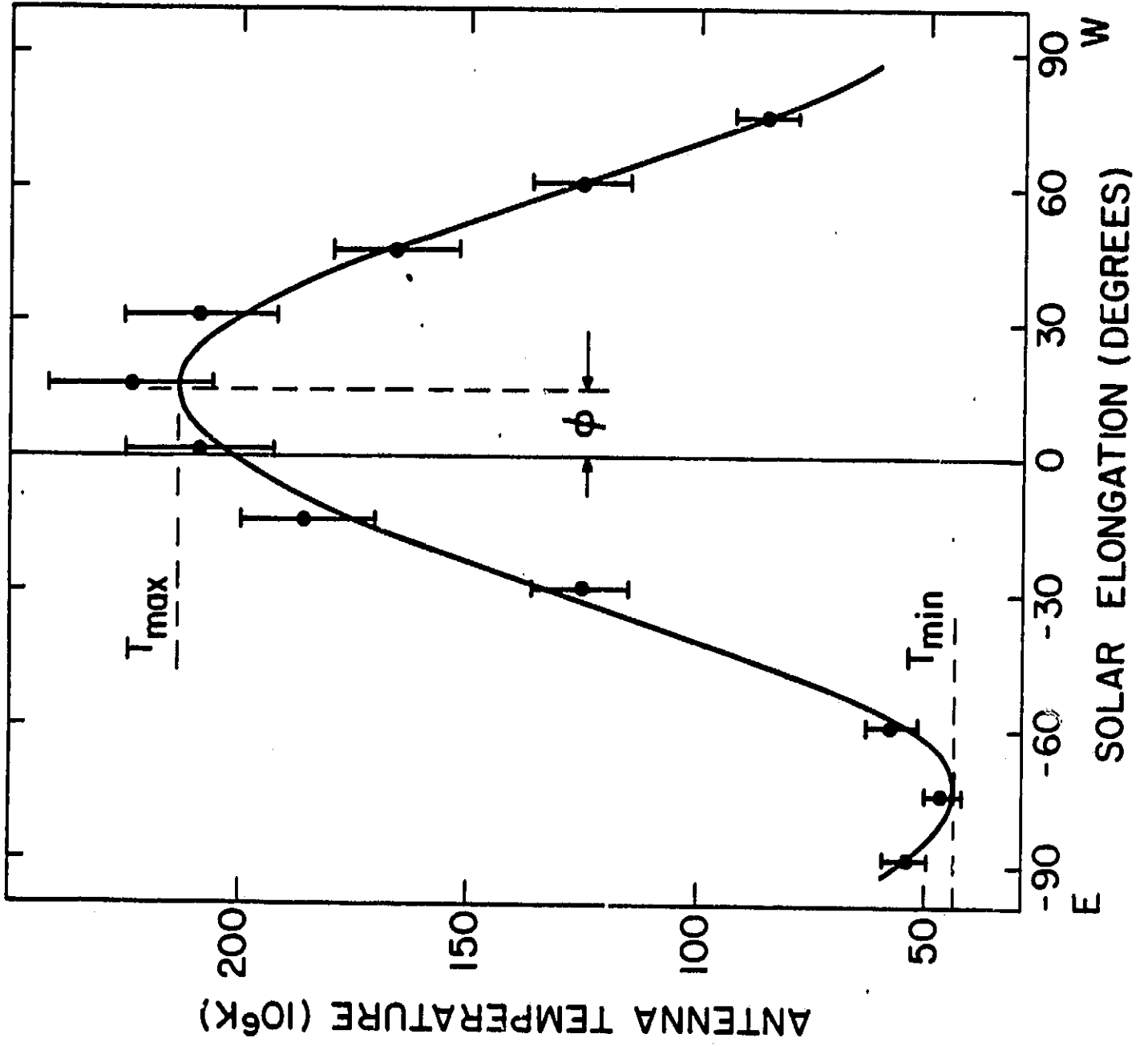
Solar elongation of the modulated Galactic background component measured during quiet periods. The straight line is least-squares fitted and is used to determine the Galactic background direction at any time.

TABLE 1

Type III storm	Measured on	Range (AU)	Density Scale ( $\text{cm}^{-3}$ ) (R in AU)	Extrapolated Enhancement(*) /HELIOS model at		Average S. Wind Speed ( $\text{km s}^{-1}$ )
				0.1 AU	1.0 AU	
May 31-June 7, 1979	June 3-5	0.06-0.46	12.8 $R^{-2.37}$	3.9	2.1	270
June 11-18, 1979	June 14-16	0.09-0.48	9.4 $R^{-2.81}$	7.8	1.2	300
Jan 3-8, 1980	Jan 4-7	0.05-0.80	17.4 $R^{-2.21}$	3.6	2.8	590
Dec 26-29, 1980	Dec 27-28	0.09-0.53	2.5 $R^{-3.98}$	30.3	0.4	250
HELIOS 1-2 data 1976 normalized (Bougeret <u>et al.</u> , 1983c)	1974-1980	0.30-1.00	6.14 $R^{-2.10}$	1.0	1.0	

(\*) assuming radiation on the harmonic of the plasma frequency.

FIGURE 1





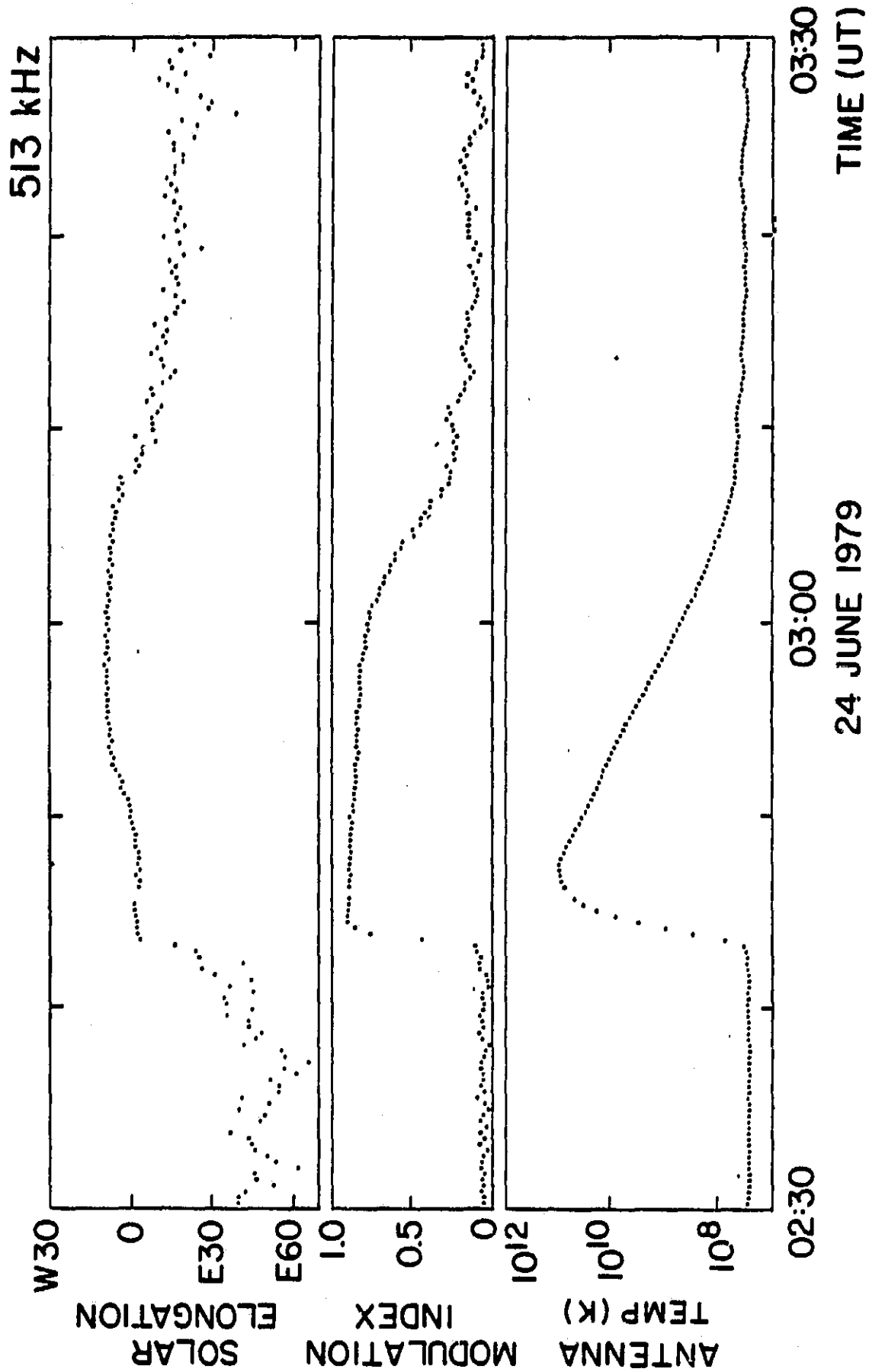


FIGURE 2

INTERPLANETARY TYPE III STORM (ISEE-3 RADIO EXPERIMENT)

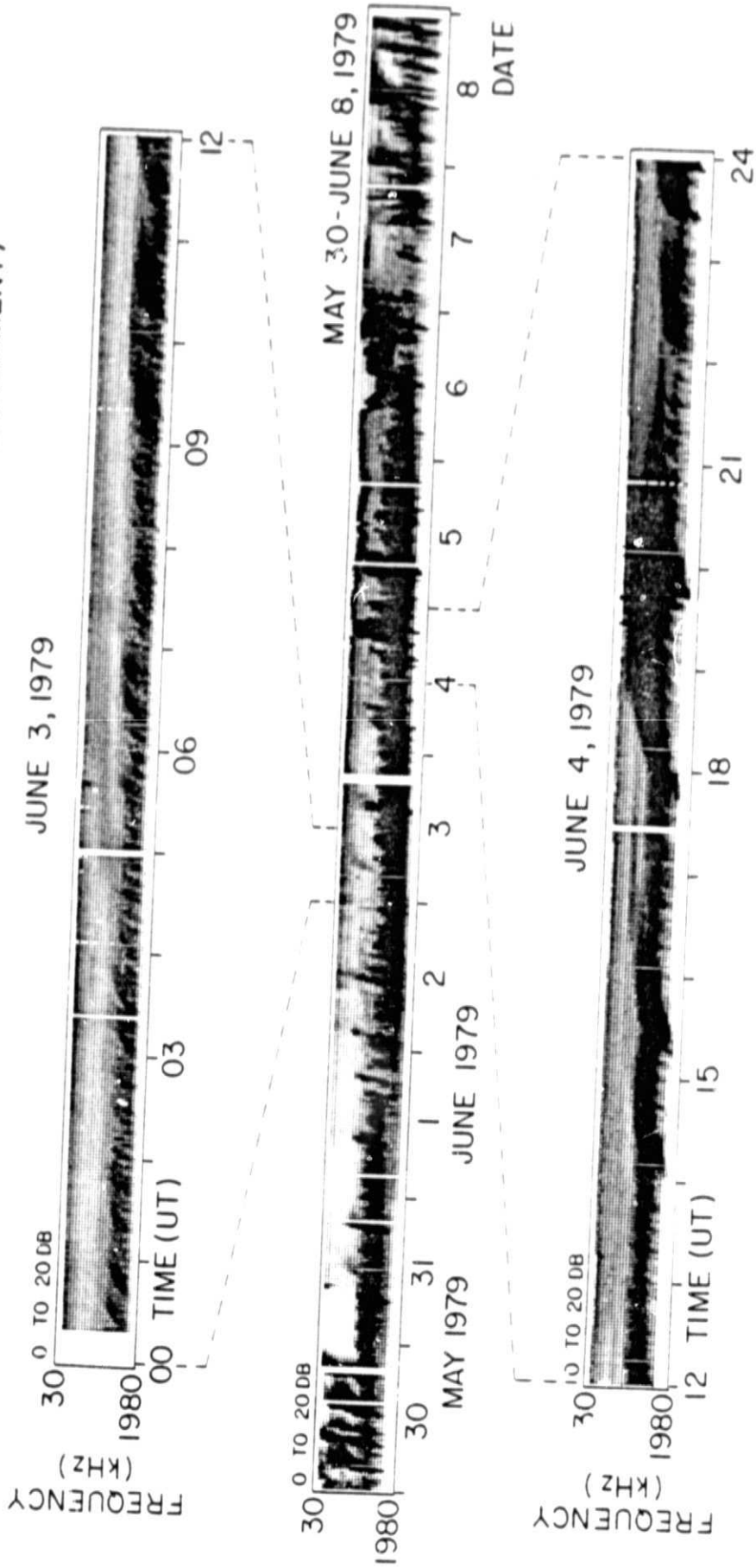


FIGURE 3

# ISEE-3 RADIO EXPERIMENT

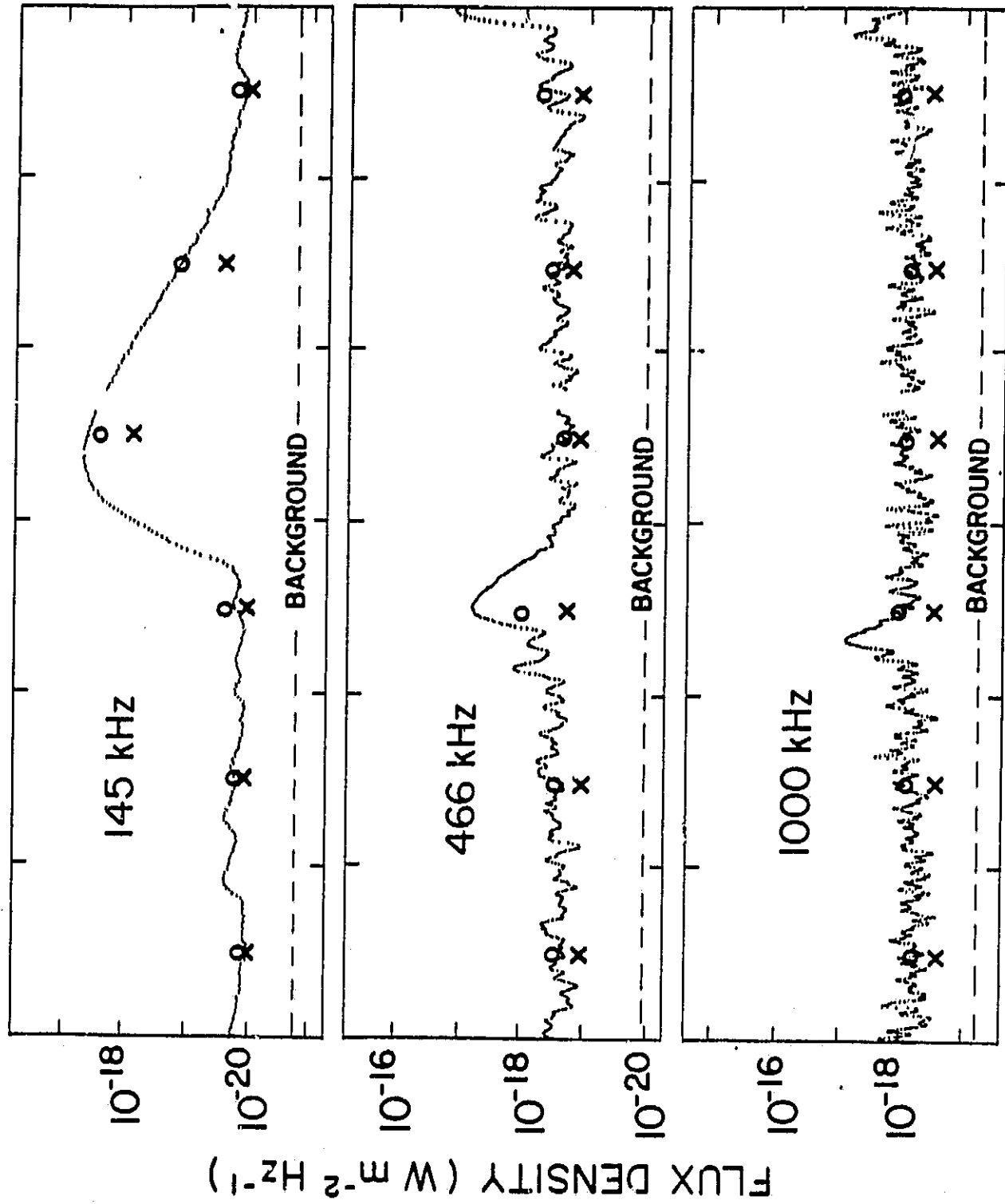


FIGURE 4

09:00 UT      10:00      11:00      12:00

2 JUNE 1979

# INTERPLANETARY STORM (ISEE-3 RADIO EXPERIMENT)

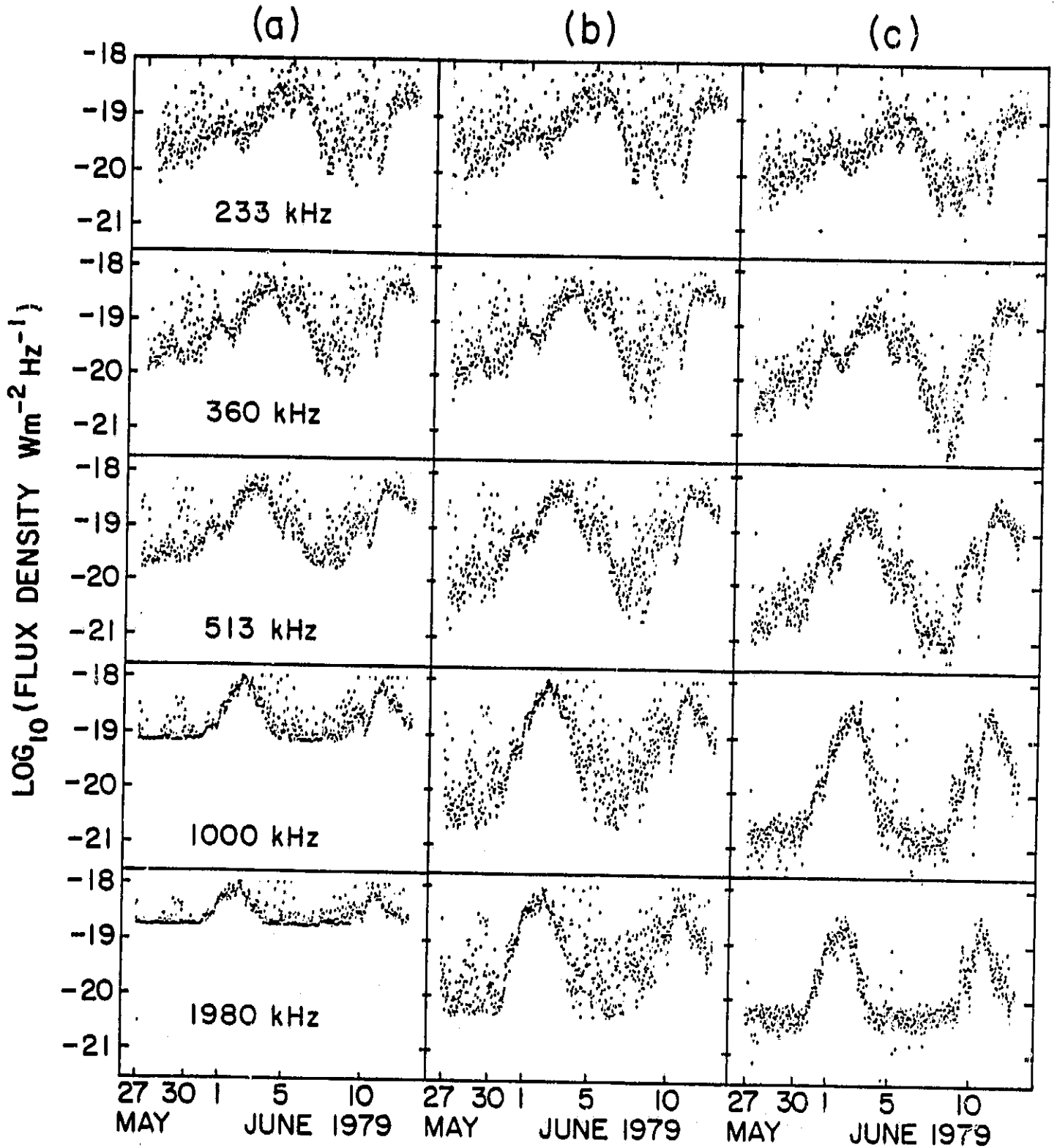


FIGURE 5

# ISEE-3 RADIO EXPERIMENT

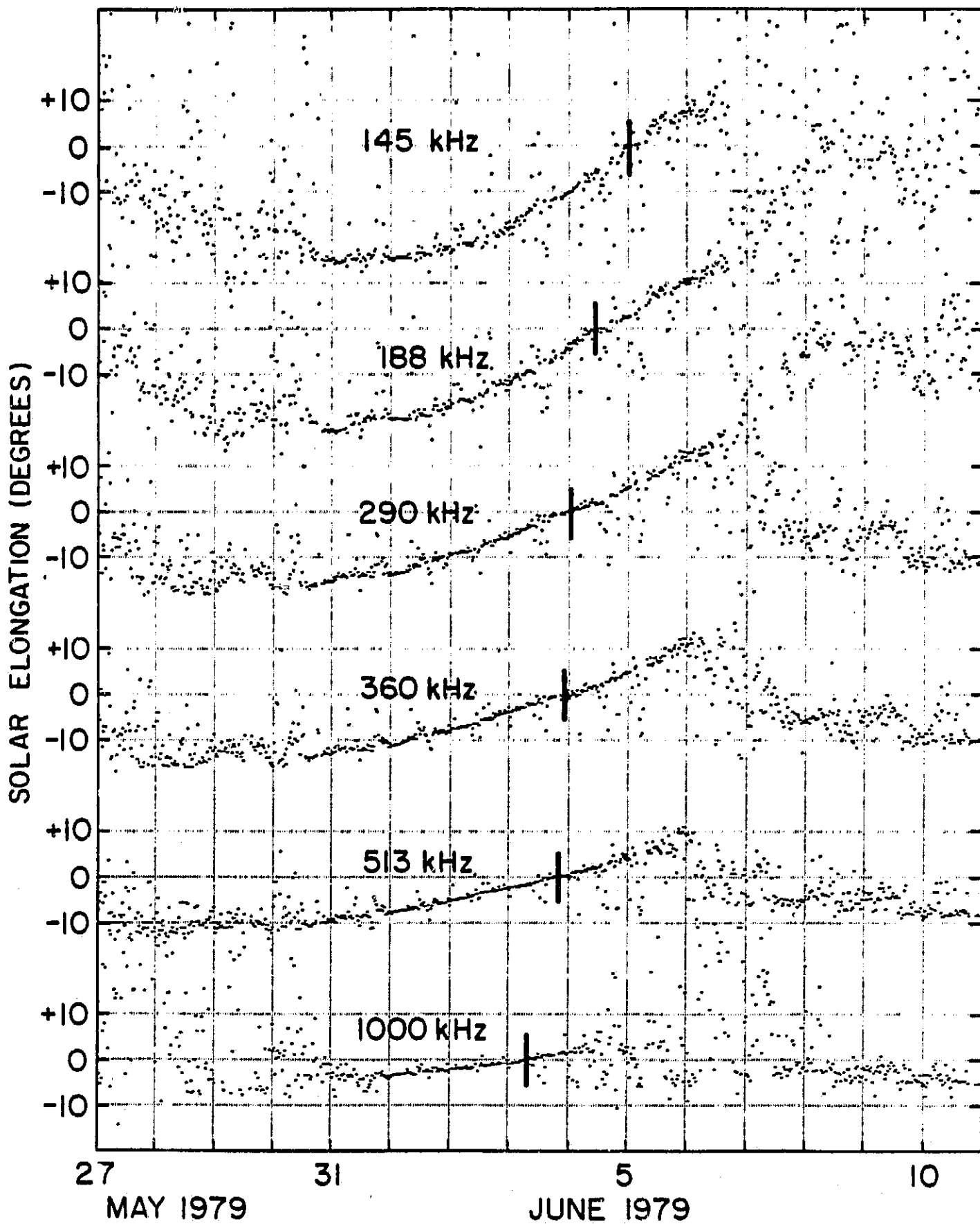


FIGURE 6

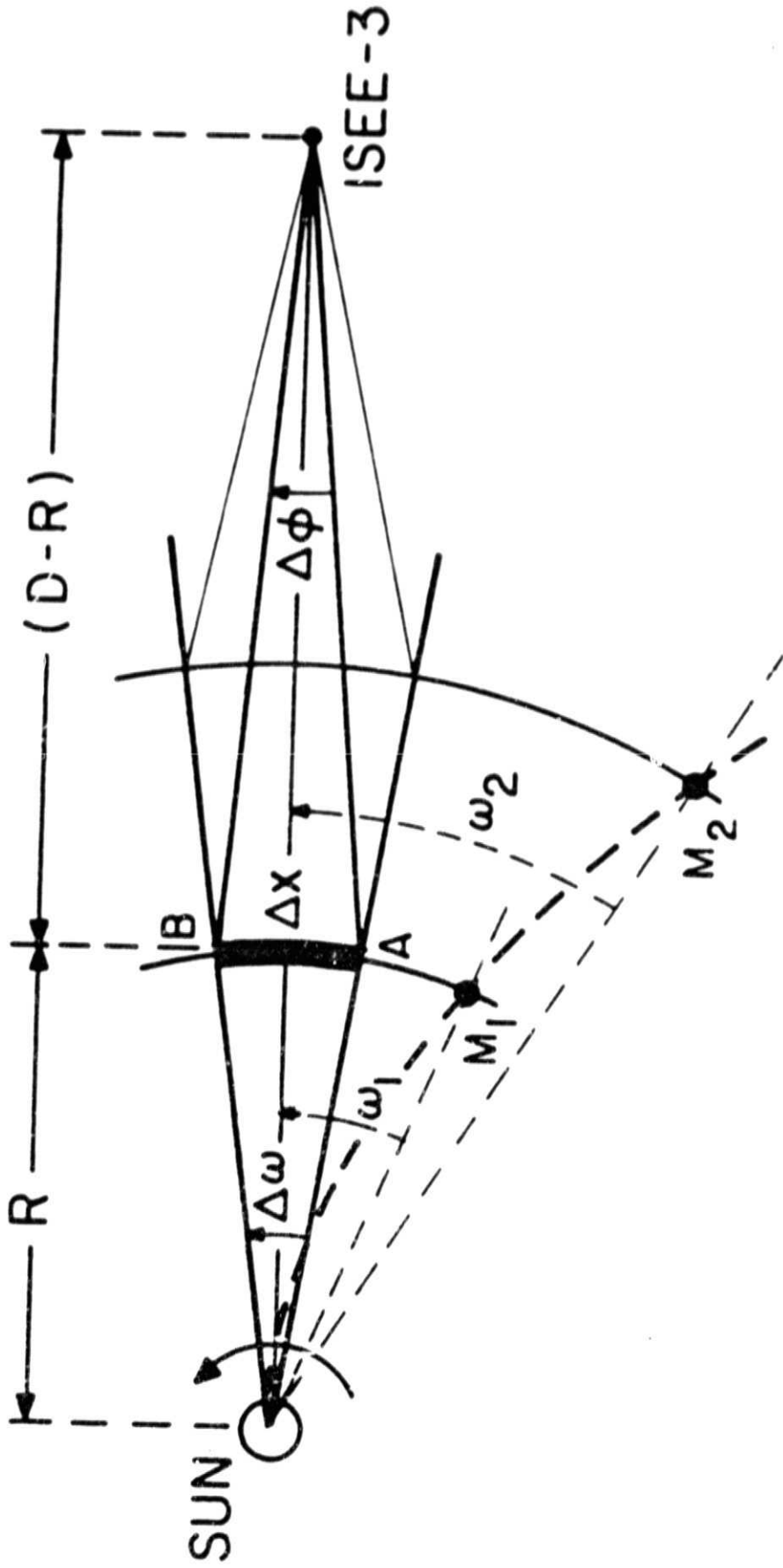


FIGURE 7

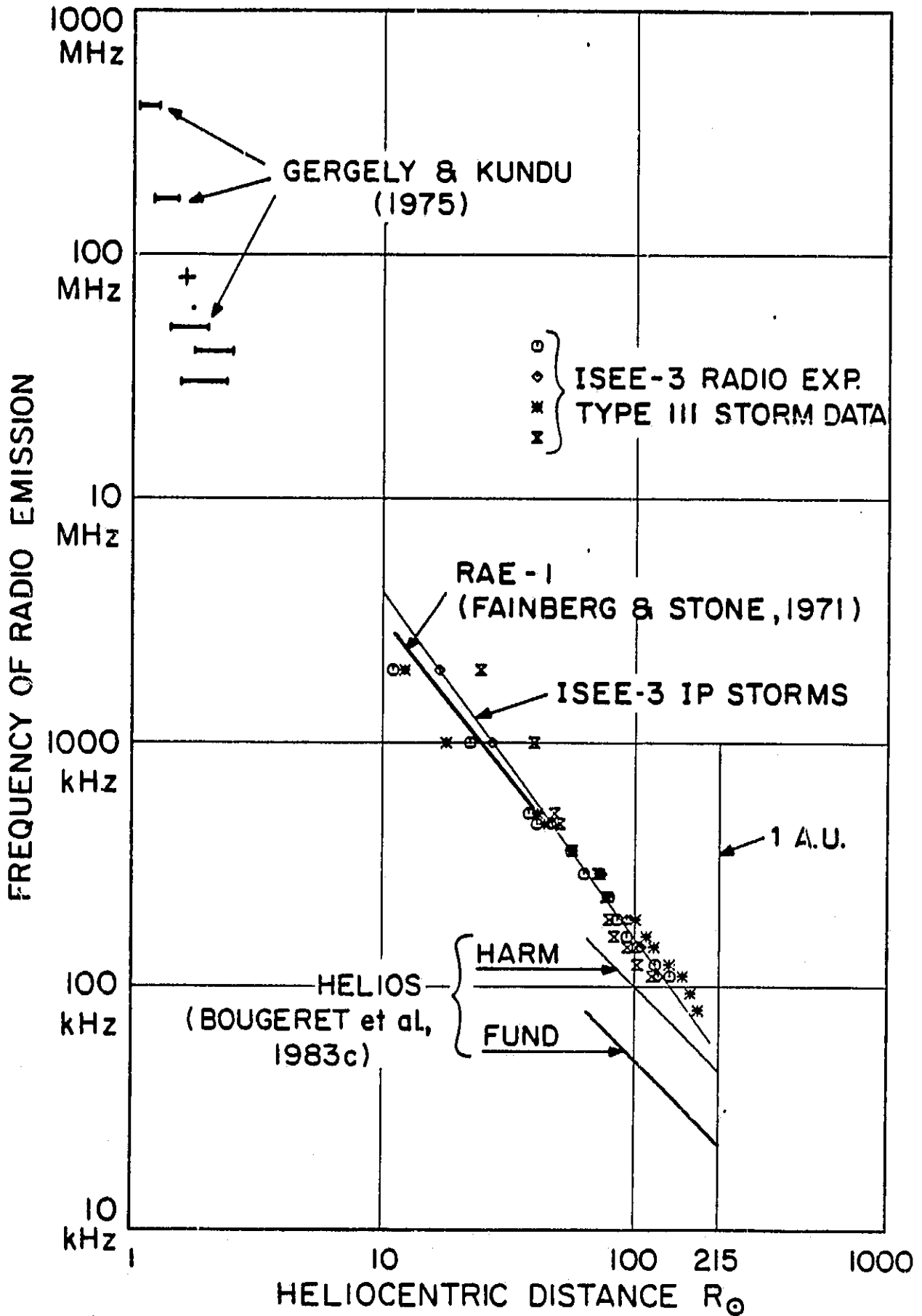


FIGURE 8

IP TYPE III STORM  
JUNE 3-5, 1979

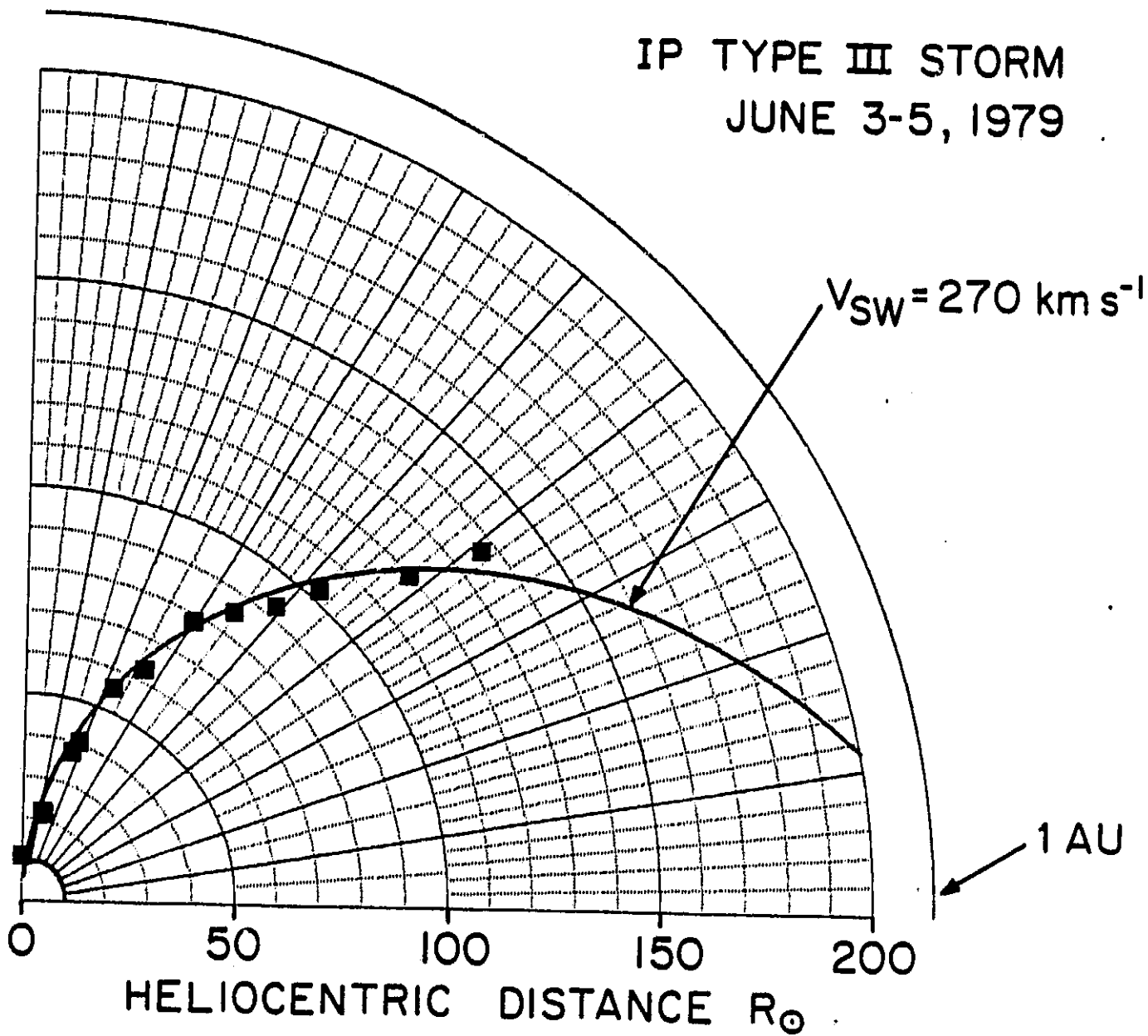


FIGURE 9



# IP STORM (ISEE-3)

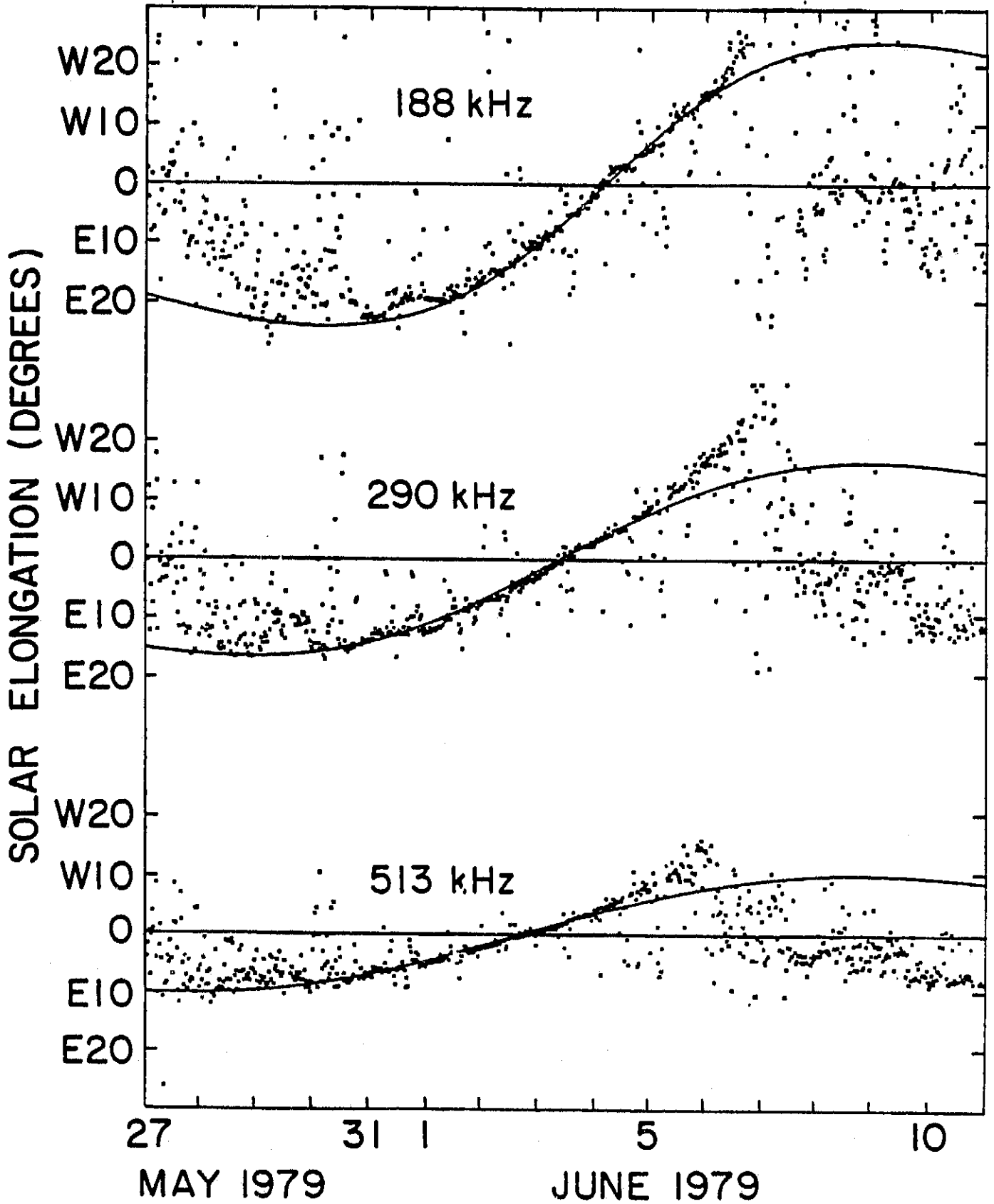


FIGURE 10

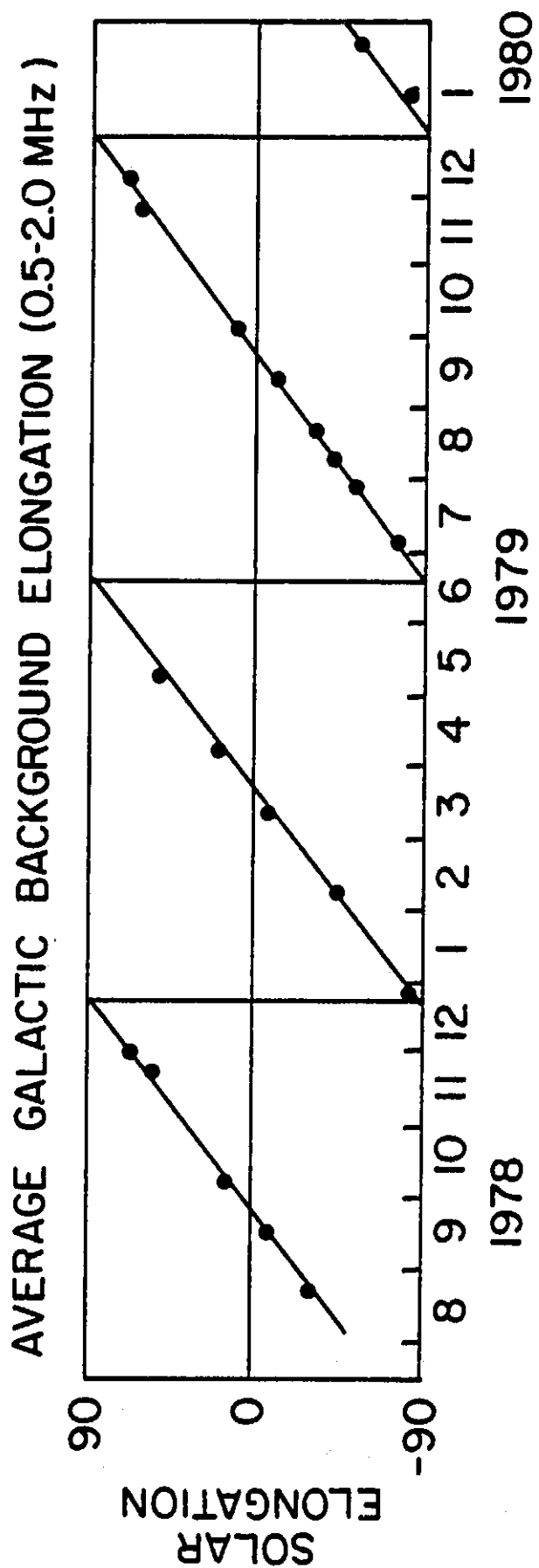


FIGURE A1